Electron microscopy of phase transformations in $1T$-TaS_2

Takashi Ishiguro* and Hiroshi Sato
School of Materials Engineering, Purdue University, West Lafayette, Indiana 47906
(Received 1 October 1990; revised manuscript received 14 February 1991)

Phase transformations in $1T$-TaS_2, both on cooling from the incommensurate (IC) phase and on warming from the commensurate (C) phase are investigated by transmission electron microscopy. The transformations are strongly hysteretic, and so proper care is required in the temperature cycle of observation in order to obtain consistent results. Our results revealed that, in the intermediate region between the IC phase and the C phase [or the noncommensurate (NC) phase], the character of the transformation is different on cooling from the IC phase and on warming. On cooling from the IC phase, the structure of the NC phase essentially remains incommensurate in the basal plane and only the rotation of modulation direction occurs. However, on warming from the C phase, a discommensuration structure composed of small domains with the structure of the C phase appears. These domains are separated by a discommensuration network whose density changes with temperature. As a result, both the rotation of diffraction spots around the c axis and the decrease of the averaged period with increasing temperature occur by this mechanism. High-resolution images for both the C phase and the NC phase are taken in a direction parallel to the c axis as well as perpendicular to the c axis. Details of the change in the stacking order during the transformation process are thus revealed.

I. INTRODUCTION

$1T$-TaS_2, which shows complicated features of phase transformations involving the formation of charge-density waves (CDW), has attracted many researchers.[1,2] The material is basically a quasi-two-dimensional metal like $2H$-$TaSe_2$, whose behavior has been investigated extensively.[3–7] But because of its symmetry, the characteristics of the transformations are not confined to two dimensions and there are additional complicating features. The modulated structure shows an incommensurate-commensurate phase transformation, which involves not only a change in the period of modulation such as that observed in $2H$-$TaSe_2$,[3–7] but also a change in the angle of modulation direction relative to the fundamental structure. The phases which are involved in the transformation that have been identified are the normal (N)($T > 543$ K, $P\bar{3}m$, without CDW), the incommensurate (IC) ($354K \leq T \leq 543K$), the noncommensurate or nearly commensurate (NC) ($183\ \text{K} \leq T \leq 353$ K) and the commensurate (C) ($T \leq 183$ K).[8] In addition, on warming from the C phase, the existence of an anomaly at about 280 K in several physical properties such as thermal expansion,[9] He^+-ion channeling,[10] Young's modulus,[11] electrical resistivity,[12] the Seebeck coefficient,[12] and specific heat,[13] suggests the existence of yet another phase in the NC region. Fung, Steeds, and Eades[14] studied the stacking order of this structure by convergent-beam electron microscopy and showed that, below this temperature, the stacking period changes to $7c_0$, which is different from the $3c_0$ of the NC phase. In view of this change, Tanda *et al.*[15] further investigated this anomaly and found another phase on warming from ~200 to 280 K. The structure is triclinic and incommensurate, and is called the T phase. The existence of hysteresis, hence the difference between the behavior on cooling and warming, and the existence of the T phase on warming from the C phase have been experimentally observed. Due to the existence of such a strong hysteresis, the data depend on the thermal history. Inconsistencies among earlier data that did not account for the hysteresis have led to much confusion.

Earlier, McMillan studied the incommensurate-commensurate transitions by the Landau phenomenological theory of phase transitions and proposed the concept of discommensuration, which involves the incommensurate-commensurate phase transition.[16] Based on this concept, Nakanishi and Shiba[17] proposed a discommensurate network model in the basal plane of the NC phase of $1T$-TaS_2. Additional attempts to understand the discommensurate structure of the NC phase have also been made.[18,19] Experimental confirmations of the discommensurate state, such as that proposed by Nakanishi *et al.*,[17] have been a goal in the study of $1T$-TaS_2.

Tanda *et al.* carried out an x-ray experiment on the T phase, taking the NC phase as an initial state, and showed a deviation from the threefold symmetry in the basal plane.[15] The result was analyzed by a discommensuration network model.[20] Their result seemed to be supported by a scanning tunneling microscopy (STM) investigation of $1T$-TaS_2 by Thomson *et al.*, which shows the discommensurate structure in the T-phase.[21]

In addition to the above observations that the discommensurations appear only in the warming stage, there is also evidence in more precise measurements of the specific heat, resistivity, and Hall coefficient by Bayliss, Ghorayeb, and Guy which suggests that the NC phase observed during cooling from the IC phase is not the same as the NC phase observed on warming from the C

phase.[22] Moreover, the thermal-expansion data taken by Sezerman, Simpson, and Jericho[9] show a strong anomaly in the interlayer interaction on warming from the C phase as compared to that on cooling from the IC phase. These data clearly show that, in order to investigate the mechanism of the transformation, it is most important to allow for effects due to the temperature hysteresis of the transformation, and to obtain consistent data on cooling and on warming.

High-resolution electron microscopy has proved to be a very powerful technique for developing an understanding of incommensurate-commensurate transition and discommensurations.[3–7] Because of difficulties in obtaining high-resolution images at low temperatures,[6,7] and due to the existence of the temperature hysteresis, a systematic high-resolution electron microscopy has not been undertaken until now, when we decided to re-examine phase transitions in $1T$-TaS_2 by means of high-resolution electron microscopy. In view of the thermal hysteresis, we always started from the well-annealed IC phase and went through a cooling and heating cycle via the C phase each time the experiment was conducted. We found that we could obtain reproducible and reliable results necessary for an understanding of the mechanism of the transformation by the above procedure.

Observations were made both perpendicular to the c axis as well as parallel to the c axis. This reveals directly the change of the stacking order with temperature. We thus confirmed by electron microscopy that no discommensuration was involved in the incommensurate-commensurate transformation on cooling from the IC phase, but that the discommensurate state appears on warming from the C phase. We also concluded that the T phase was a discommensurate state with stacking order intermediate between that of the C phase and the $3c_0$ of the NC phase. At $\sim$280 K on warming, we could observe a sudden change of the stacking order to $3c_0$, which explained the existence of the anomaly in physical properties at this temperature.[9,13] On warming from the C phase, the NC phase was also in a discommensurate state and, hence, the NC phase on cooling from the IC phase and on warming from the C phase were essentially different. On the basis of this observation, an idealized model of discommensuration has been constructed which could explain the experimental results.

II. EXPERIMENT

The observations were made by a JEOL 2000 FX electron microscope with a point-to-point resolution of 0.29 nm and a vacuum of 0.7×10^{-5} Pa by ion-pump evacuation. Low-temperature observations were made by a double-tilt liquid-helium specimen holder (Gatan, Ltd.) that could realize a stable temperature condition by controlling the heater current. Either liquid nitrogen or dry ice was used as a coolant material. The dry ice was found to be very effective, especially for observations above 210 K because of the absence of bubbling and also because of its large latent heat of vaporization. A double-tilt heating holder, EM-SHTH (JEOL Ltd.), was also used for high-temperature observations. All high-resolution images were taken using the computer-controlled minimum dose system method which enabled us to catch exposure timing under driftless condition without any radiation damage while focusing on areas of interest in the specimen. Single crystals of $1T$-TaS_2 were grown by means of a vapor transport technique, using I_2 gas as a transport agent, at the Central Material Preparation Facility of Purdue University.

Two different types of TEM specimens were prepared as follows. To prepare specimens for observation parallel to the c axis, crystals were cleaved along the basal plane and mounted on copper meshes by silver epoxy glue (EPO-TEK H20E). To prepare specimens for observation perpendicular to the c axis, crystals were sandwiched between MgO single crystals by epoxy glue and these were mechanically polished to the thickness of about 100 μm using SiC powder. These thin plates were then attached to Rh-coated copper single-hole meshes by silver epoxy glue and ion-thinned by means of a Dual Ion Mill model 600 (Gatan, Ltd.) using Ar gas at liquid-nitrogen temperature. This enabled us to suppress the phase transformation from the $1T$ structure to the $2H$ structures[23] caused by the increase of specimen temperature due to ion bombardment.

III. RESULTS

A. Temperature variation of a diffraction pattern projected on the basal plane

For a general picture of the phase transitions, the temperature dependence of the projection of the fundamental modulation wave vectors $\mathbf{q}_1$, $\mathbf{q}_2$, and $\mathbf{q}_3$ on the basal plane will be explained first. The relations between $\mathbf{q}_1$, $\mathbf{q}_2$, and $\mathbf{q}_3$ and their projections on the basal plane, $\mathbf{q}_1^P$, $\mathbf{q}_2^P$, and $\mathbf{q}_3^P$, are shown in Fig. 1(a). There, secondary reflections are those specified by $\mathbf{q}_1-\mathbf{q}_2$ (i.e., $\mathbf{q}_1-\mathbf{q}_2$, $\mathbf{q}_2-\mathbf{q}_3$, and $\mathbf{q}_3-\mathbf{q}_1$). The vectors (1,0,0) and (0,1,0) represent the $\mathbf{a}^*$ and $\mathbf{b}^*$ axes, respectively, which are the fundamental reciprocal lattice vectors in the basal plane for the fundamental structure of $1T$-TaS_2, and these define the unit cell of the normal (N) structure in reciprocal space. The projections $\mathbf{q}_1^P$, etc., and $\mathbf{q}_1^P-\mathbf{q}_2^P$, etc., are shown in Fig. 1(b). The symbols IC, NC, and C indicate the respective phases involved in the transformation. Based on Fig. 1(b), the angle ϕ indicates the deviation of $\mathbf{q}_1^P$ from the $\mathbf{a}^*$ axis.

In Figs. 2 and 3, the temperature dependences of ϕ and $|\mathbf{q}|^P/|\mathbf{a}^*|$ are plotted, where $|\mathbf{q}^P|$ is the averaged length of the projections of $\mathbf{q}_1^P$, $\mathbf{q}_2^P$, and $\mathbf{q}_3^P$. These data are calculated by measuring the relative distances between secondary reflections in [001] diffraction patterns taken precisely with a precise camera length 250 cm. Such plots have been used by Scruby, Williams, and Parry,[8] but without accounting for the hysteresis with temperature. In taking the present data (and also for observing the high-resolution images) the specimen was first kept at 375 K (in the IC phase) for more than 1 h, and then the specimen was allowed to go through the necessary thermal history to reach the desired state. With use of this process, the reproducibility of the data taken was found to be

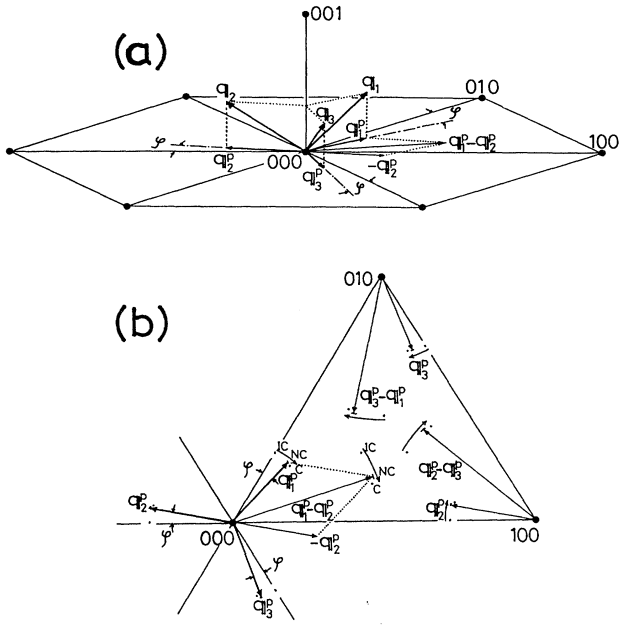

FIG. 1. (a) Schematic view of the primary diffraction vectors ($\mathbf{q}_1,\mathbf{q}_2,\mathbf{q}_3$) and their projections ($\mathbf{q}_1^P,\mathbf{q}_2^P,\mathbf{q}_3^P$) on the basal plane. 100 and 010 correspond, respectively, to the $\mathbf{a}^*$ and $\mathbf{b}^*$ of the normal (N) structure. (b) Projection of the diffraction spots on the basal plane and the definition of angle ϕ.

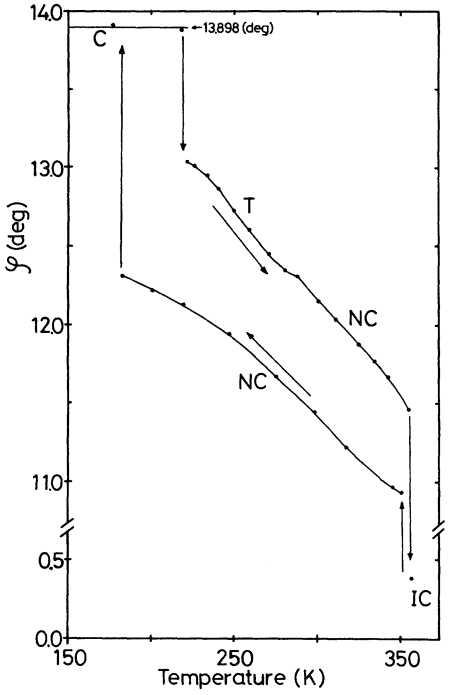

FIG. 2. Temperature dependence of ϕ. A large hysteresis can be seen along one cycle of temperature change between the IC phase and the C phase. An anomaly at around 280 K at $\phi=12.3°$ between the T phase to the NC phase on warming should be noted.

very good. In some cases, when diffraction patterns are recorded by lowering the temperature step by step, the NC phase was not found to transform to the C phase on cooling. A possible reason for this phenomenon might be the radiation damage caused by electron beam, as has been mentioned by other investigators.[24,25]

Figure 2 shows the temperature dependence of the angle ϕ relative to the fundamental reciprocal lattice. The measured angle for the C phase, 13.898°, is in good agreement with the calculated angle of $\tan^{-1}(\sqrt{3}/7)$ within an experimental error of ±0.02°. The angle for the IC phase is 0.38° at 357 K. This means that the projected direction of the primary spot of the IC phase is not exactly directed towards the shortest fundamental reciprocal-lattice vector in the basal plane as was first pointed out by Van Landuyt.[23] The transition temperatures (IC↔NC; NC↔C) shown in Fig. 2 are consistent with those reported by other investigators.[24] The most important behavior in this figure is that there is a large hysteresis in the transformation between the IC phase and the C phase. The angle ϕ in the NC phase, on cooling, gradually increases after a discontinuous jump at ~347 K from that of the IC phase, and, at around 12.3°, jumps to that of the C phase at ~183 K. On warming, ϕ changes discontinuously from the C phase to the NC phase at ~223 K and to the IC phase at ~354 K. Between these two transformations, the variation of ϕ is continuous, but there is an anomaly at around 280 K, at which temperature ϕ is ~12.3°. On the basis of previous observations, these two phases separated by the kink at 280 K are believed to be the T phase and the NC phase, respectively. It should, however, be mentioned that the variation of ϕ with temperature in the NC phase on cooling from the IC phase and that on warming from the C phase are different.

Figure 3 shows the temperature dependence of the length of the projected primary spots $|\mathbf{q}^P|$ relative to the $|\mathbf{a}^*|$, i.e., $|\mathbf{q}^P|/|\mathbf{a}^*|$ in the basal plane. There is also a large hysteresis. The agreement between the measured

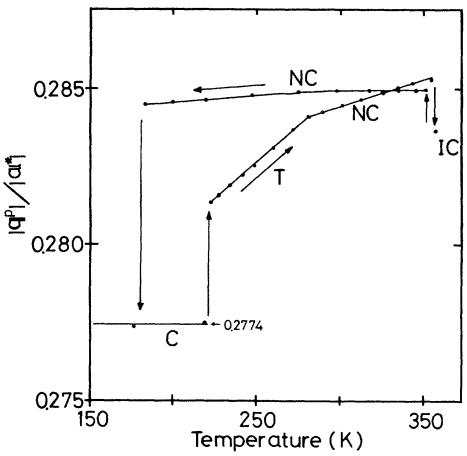

FIG. 3. Temperature dependence of $|\mathbf{q}^P/|\mathbf{a}^*|$. Note the change of slope at ~280 K between the T phase and the NC phase on warming.

values, 0.2774, and the calculated one, $1/\sqrt{13}$, in the C phase is within an error of $\pm 0.000\,15$. On cooling, $|\mathbf{q}^P|/|\mathbf{a}^*|$ of the NC phase decreases with temperature a little, but its temperature coefficient is very small compared to that for warming. On warming from the C phase, there is a clear bend in the temperature coefficient at ~ 280 K which separates the T phase and the NC phase. But, within the T phase and the NC phase, the temperature coefficients are almost linear. However, the temperature coefficient in the T phase is larger than that in the NC phase.

Combination of these two relations (Figs. 2 and 3) indicates that, in the NC phase on cooling from the IC phase, the change corresponds to that of a pure rotation, whereas, in the T phase and in the NC phase on warming from the C phase, both the rotation and the increase of the length of the modulation wave-number vector in the basal plane occur at the same time. In other words, the NC phase on cooling has a character close to the IC phase and practically no discommensuration takes place, while in the T phase and in the NC phase on warming from the C phase, a discommensuration process takes place.

Before describing these phases in detail, we would like to show a series of [001] diffraction patterns in Fig. 4, which corresponds to one thermal cycle starting from the IC phase. The inset in each diffraction pattern is an enlargement of a secondary spot indicated by an arrow. The intensity of the secondary spots of the IC phase [Fig. 4(a)] is usually rather weak. The intensity distribution of any of these spots in the basal plane has an elliptical shape elongated towards the azimuthal direction with the origin at the fundamental spot. On cooling from the IC phase, the secondary spots in the NC phase [Figs. 4(b) and 4(c)] have a disk-shaped intensity distribution. Also, the intensity of the secondary spots in the high-temperature region [Fig. 4(b)] is weaker than that in the low-temperature region [Fig. 4(c)] as pointed out by Nakanish *et al.*[18] In the C phase [Fig. 4(d)], each spot also has a disk-shaped intensity distribution including the primary spots. Figure 4(e) shows a diffraction pattern taken at the transition temperature from the C phase to the T phase on warming. There is a small separation between the secondary spots of the C phase and those of the T phase, and the direction of this separation is different from that expected from the structure of the T phase reported by Tanda *et al.*[15,20] Figure 5 compares the present experiment and that of Tanda *et al.* with respect to the locations of the secondary reflections projected on the basal plane. Intersections of fine lines in the triangle $(0\mathbf{a}^*\mathbf{b}^*)$ correspond to the positions for the reflections of the C phase. Solid circles $\mathbf{q}_1^P-\mathbf{q}_2^P$, $\mathbf{q}_2^P-\mathbf{q}_3^P+\mathbf{a}^*$, and $\mathbf{q}_3^P-\mathbf{q}_1^P+\mathbf{b}^*$ are positions for the reflections of the present experiment and correspond to the diffraction pattern shown in Fig. 4(e). On the other hand, open circles $\mathbf{Q}_1-\mathbf{Q}_2$, $\mathbf{Q}_2-\mathbf{Q}_3+\mathbf{a}^*$, and $\mathbf{Q}_3-\mathbf{Q}_1+\mathbf{b}^*$ are positions for the reflections obtained by calculation from the paper of Tanda *et al.* (Here $\mathbf{a}^*$ and $\mathbf{b}^*$ are interchanged in the calculation so that ϕ may be represented in an identical fashion in both experiments.) Based on the fact that relative locations of the three secondary reflections from the C phase are asymmetric, Tanda *et al.* proposed a stretched domain model for the T phase. However, the model is not supported by the present experiment, as is clear from the diffraction pattern in Fig. 4(e).

The character of the diffraction pattern of the T phase [Figs. 4(f) and 4(g)] is that the secondary spots have deformed elliptical intensity distributions. These spots

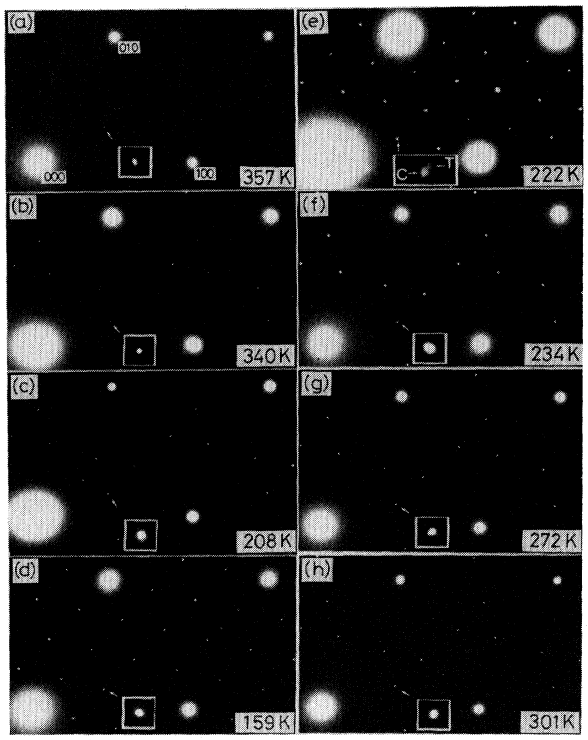

FIG. 4. Temperature variation of the [001] diffraction patterns: (a) the IC phase, (b) and (c) the NC phase on cooling, (d) the C phase, (e) at the transition point from the C phase to the T phase. The splittings of the secondary spots due to the coexistence of the C phase and the T phase are seen. (f) and (g) show the T phase, (h) the NC phase on warming.

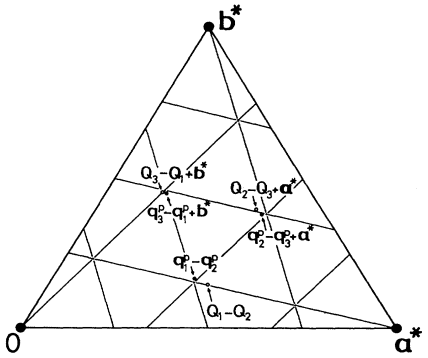

FIG. 5. Comparison of the locations of the secondary reflections projected on the basal plane of the present experiment with those of Tanda and Sambongi (Ref. 20).

seem to be elongated toward the direction of the change of $|\mathbf{q}^P|/|\mathbf{a}^*|$ and ϕ with temperature of the T phase. This character is not affected by the rate of temperature change from the C phase and does not change by keeping the temperature constant. The locations of the center of gravity in the intensity distribution of those secondary spots are different from those of the C phase. The deformation of the intensity distribution of diffraction spots of the T phase becomes smaller with increasing temperatures. In the NC phase on warming from the C phase [Fig. 4(h)], diffraction patterns with secondary spots having disk-shaped intensity distributions reappear which are similar to those in the NC phase on cooling from the IC phase.

B. Phase transition from the IC phase to the NC phase on cooling

An observation by means of electron microscopy of the phase transformation between the IC phase and the NC phase on cooling made by Van Landuyt, using a dark field imaging technique,[23] showed successive changes in the domain distribution of the IC and NC phases during the transformation. There is a large difference in ϕ between the IC phase and the NC phase as shown in Fig. 2. In order to see this transformation, we took dark field images using a pair of primary spots of the IC phase and of the NC phase around the 310 fundamental spot. Figures 6(a) and 6(b) are images taken under this condition from the same area, with a temperature difference of about 3° at around the transition temperature on cooling. The coexistent region of the IC and NC phases is seen by a region with moiré fringes having a period of about 5 nm. This agrees with the calculated period of 4.8 nm by assuming $|\mathbf{q}_{IC}| = 1.1257\ \text{nm}^{-1}$, $|\mathbf{q}_{NC}| = 1.1295\ \text{nm}^{-1}$, and an angle ϕ of 10.55° between these vectors. Because a part of the moiré fringes disappears from Fig. 6(a) to Fig. 6(b), we can conclude that the NC phase is growing along the c axis. The coexistent regions of the IC and NC phases with moiré fringes show almost straight borderlines having edges making about 120°. This means that the NC phase grows in the c plane towards the direction parallel to one of the wave vectors ($\mathbf{q}_{2NC}$) and the direction perpendicular to that ($\mathbf{q}_{1NC}$) as schematically shown in Fig. 7. In the IC and NC regions, there are some contrasts similar to those of edge dislocations indicated by arrows in Fig. 6. These defects do not seem to be related to this transformation mechanism as these dislocations do not move during the transformation.

Figure 8 shows a diffraction pattern taken under the 400 Bragg excitation condition by tilting the specimen, which shows diffuse streaks of the spots from the IC

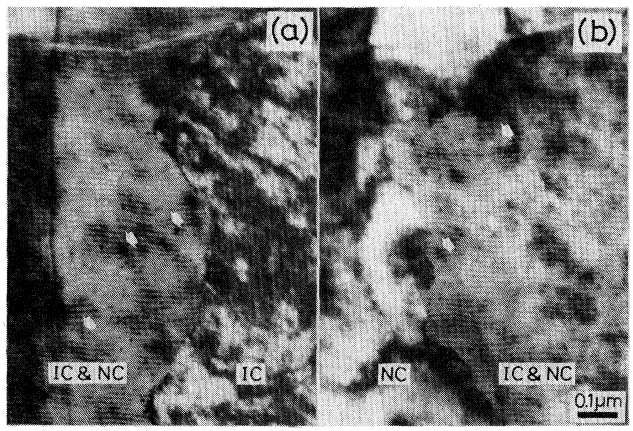

FIG. 6. Dark field images of the phase transformation from the IC phase to the NC phase on cooling. Both (a) and (b) represent the same region. The temperature of (b) is lower than the temperature of (a) by 3°. Because a pair of primary spots of the IC phase and the NC phase are used, the region with moiré fringes corresponds to the coexisting region of the IC phase and the NC phase on cooling.

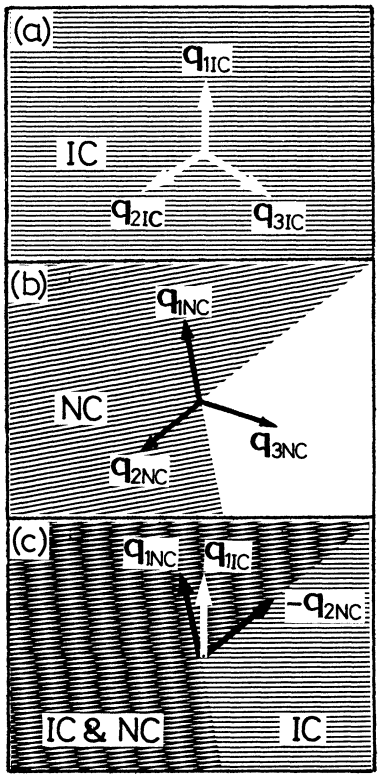

FIG. 7. Explanation of the appearance of moiré fringes and of the direction of growth when the NC phase grows from the IC phase. (a) $\mathbf{q}_{iIC}$ ($i=1,2,3$) is the primary reflection vector of the IC phase. The lateral stripe shown is that corresponding to $\mathbf{q}_{1IC}$. (b) $\mathbf{q}_{1NC}$'s make an angle of $\sim 10°$ with respect to $\mathbf{q}_{1IC}$'s. The stripes shown correspond to $\mathbf{q}_{1NC}$. The region of the NC phase has boundaries parallel to $\mathbf{q}_{1NC}$ and $\mathbf{q}_{2NC}$. (c) Superposition of (a) and (b) and the appearance of the moiré finges. The moiré fringes have the wave vector $q_{1NC} - \mathbf{q}_{1IC}$. The region with the moiré fringes is the coexistence region of the IC phase and the NC phase. The boundary between the IC phase and the region with moiré fringes makes $\sim 120°$ with respect to the IC phase, as seen in Fig. 5, indicating that the NC phase grows in a perpendicular direction to its primary reflection vectors $\mathbf{q}_{1NC}$ and $\mathbf{q}_{2NC}$.

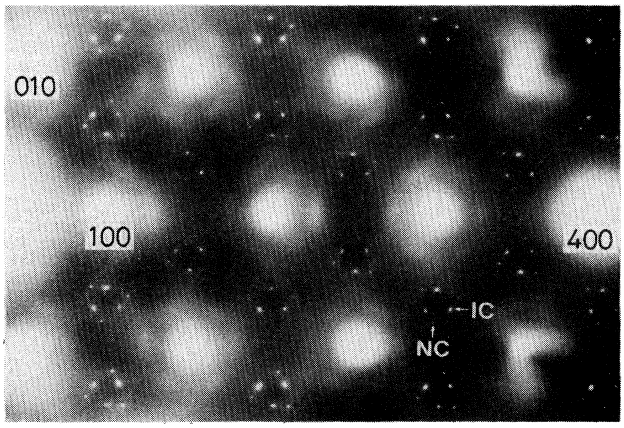

FIG. 8. Diffraction pattern under the 400 Bragg excitation condition taken at the transition temperature from the IC to the NC phase on cooling. Diffuse streaking due to the IC phase appears.

phase. There are two kinds of spots in the diffraction pattern: those from the IC phase and those from the NC phase. The secondary spots of the NC phase seem to be on the diffuse streak, which is supposed to show the Fermi surface.[1] On the other hand, the secondary spots of the IC phase seem to be off the diffuse streaking. The projection of the primary spot of both the IC phase and the NC phase are, however, on the diffuse streaks. Therefore it can be thought that both the IC phase and the NC phase are stabilized by the Fermi-surface nesting, but at different parts of the Fermi surface. The intensity distribution of secondary spots of the IC phase has an elliptical shape, whereas that for the NC phase does not. This is the reason why the moiré fringes in Fig. 6 due to the coexistence of the IC and NC phases are so wavy.

C. The NC phase on cooling

Figure 9(a) shows the [001] high-resolution image and the corresponding diffraction pattern of the NC phase on cooling taken at room temperature. The fringe contrast due to the secondary spots on the c plane is too weak to be seen clearly. Therefore, in Fig. 9(b), a processed image with enhanced secondary spots intensity is shown, in which an aperture composed of seven circles which enclose the direct beam and six secondary spots [see the inset of diffraction pattern in Fig. 9(a)] is used as the Fourier bandpass. The processed image shows the homogeneously extended fringes of hexagonal network with a local bending. Neither figure shows any evidence of discommensuration and the present result is consistent with the observations made by Kuwabara *et al.*[25]

Figure 10 shows the observation of the NC phase on cooling from the IC phase at room temperature in the direction perpendicular to the c axis, by exciting a pair of primary spots as shown in the inset. The corresponding image shows fringes which are almost straight, and the location of every third black dot aligns exactly along the c axis. The separation of primary spots from the $\mathbf{a}^*$-$\mathbf{b}^*$ plane along the c axis is also $|\mathbf{c}^*|/3$ within the experimental error. We also measured the separation of the primary spots from the $\mathbf{a}^*$-$\mathbf{b}^*$ plane along the $\mathbf{c}^*$ axis with decreasing temperature down to the C phase, expecting that the T phase, which has a stacking deviation from $|\mathbf{c}^*|/3$,[15] might appear. However, no change was observed, indicating that the T phase does not exist on cooling.

D. The commensurate phase

Figure 11 represents the diffraction pattern in the basal plane of the C phase of $1T$-TaS_2 schematically. In this figure, large solid circles correspond to the fundamental reflections and the small solid circles correspond to the spots of $\sqrt{13}\times\sqrt{13}$ superstructure. Fundamental spots coincide with some of the superstructure spots because the structure is commensurate with the normal phase at least in the basal plane. The relation between the fundamental spots and the superstructure spots is given by $3\mathbf{q}^P_{C1}+\mathbf{q}^P_{C2}=\mathbf{a}^*$. The rhombus in the figure shows the

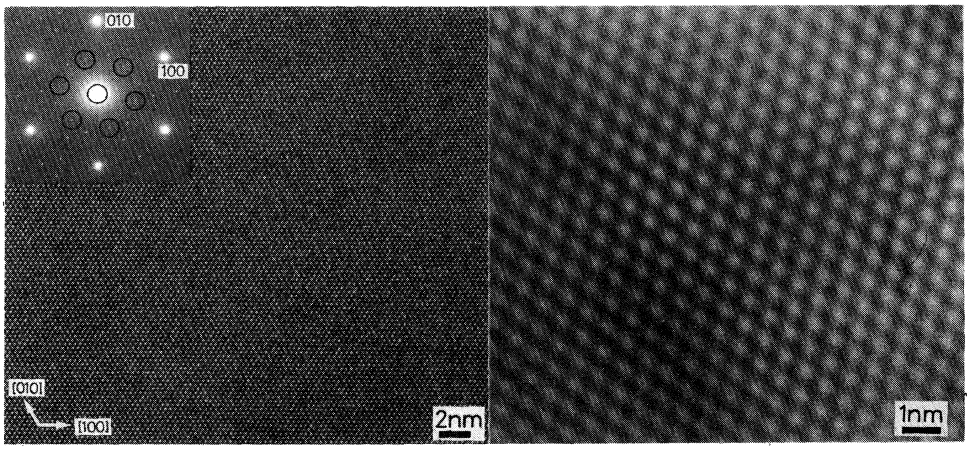

FIG. 9. (a) High-resolution image of the NC phase on cooling at room temperature with the incident beam parallel to [001] and the corresponding diffraction pattern in which the Fourier bandpass used to obtain (b) is shown by circles. In this image, weak incommensurate fringes can be seen. (b) Processed image using a direct spot and six secondary spots.

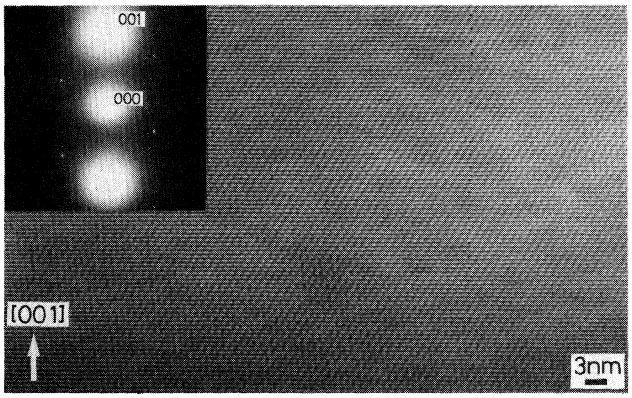

FIG. 10. High-resolution image of the NC phase on cooling at room temperature. The observed direction is perpendicular to the c axis, exciting a pair of primary spots.

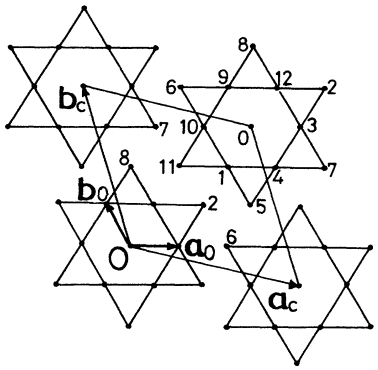

FIG. 12. The rhombus spanned by $\mathbf{a}_c$ and $\mathbf{b}_c$ is the unit cell of the C phase on one layer in the real space. A cluster of 13 Ta atoms, having the shape of the Star of David, each of which is connected by a translation vector of $-\mathbf{a}_0-\mathbf{b}_0$, belongs to the unit cell of the $\sqrt{13}\times\sqrt{13}$ structure.

unit cell in the reciprocal space in the basal plane. The corresponding unit cell in the real space is shown by the rhombus spanned by $\mathbf{a}_c$ and $\mathbf{b}_c$ in Fig. 12. Each corner of this unit cell is the site for the star-shaped cluster according to Brower and Jellinek.[26] Numbers given for the cluster indicate the possible sites for the corner of the unit cell on different stacking layers. The translation vector $-\mathbf{a}_0-\mathbf{b}_0$ (Ref. 27) gives the shift between the successive stacking layers.

Figure 13 shows a [001] high-resolution image of the C phase at 90 K and a corresponding diffraction pattern. The coarse fringes have the same period of $(\sqrt{3}/2)|\mathbf{a}_c|$ in the three independent directions, but their contrasts are different from one another, resulting in the lack of a threefold symmetry of the image. As these fringes are straight and well developed in such a wide area, it can be concluded that the C phase has the long-range order in the basal plane. The fact that the image does not have a threefold symmetry is due to the stacking disorder along the c axis, as will be mentioned later.

In order to confirm the stacking order of commensurate layers, we observed the commensurate phase from the direction perpendicular to the c axis. The specimen was kept at a temperature of 373 K for about 12 h in the TEM. This procedure is effective in eliminating the stress on the specimen induced by handling and transformations. The specimen was then cooled to 90 K to obtain the C phase. The [140] was chosen as the direction for the observation, because in this direction, the Ewald sphere not only cuts the primary reflections around the origin, but also other independent primary reflections at the same time. Such a diffraction pattern is shown in Fig. 14. In this diffraction pattern, the $h_s,0_s,\zeta$ reflections for $h_s=\pm(1,2,3,4,5)$ are elongated along the $\mathbf{c}^*$ direction. (Indices with subscript s are based on the cell spanned by $\mathbf{q}^P_{C1}$ and $\mathbf{q}^P_{C2}$. ζ is the coordinate along the $\mathbf{c}^*$ direction with the unit of $|c^*|$.) This means that, although there exists a stacking disorder, the structure in each basal plane has a long-range ordering. The $\pm 2_s,0_s,\zeta$ and $\pm 5_s,0_s,\zeta$ reflections have different intensity distribution from the others. The reason is that these reflections are

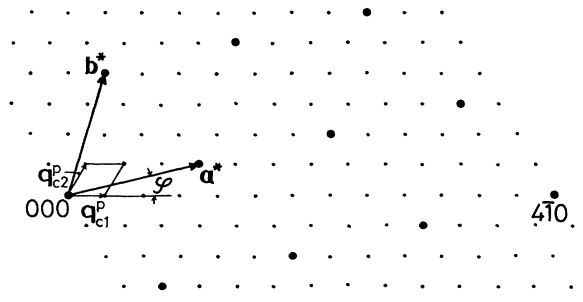

FIG. 11. Schematic diffraction pattern of the C phase in the basal plane. The rhombus spanned by $\mathbf{q}^P_{C1}$ and $\mathbf{q}^P_{C2}$ corresponds to the projected unit cell of the C phase on basal plane in reciprocal spaces.

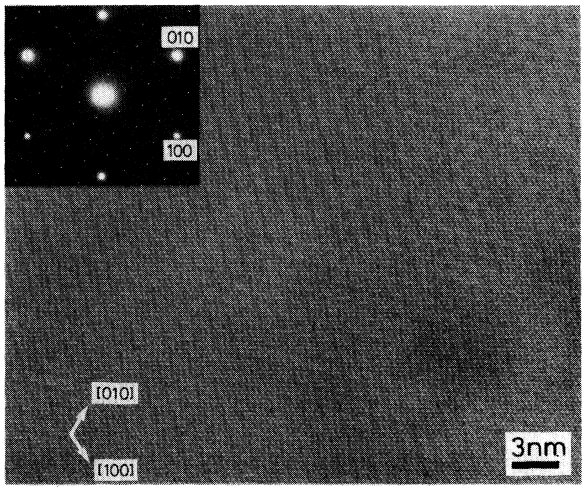

FIG. 13. [001] high-resolution image of the C phase at 90 K and a corresponding diffraction pattern.

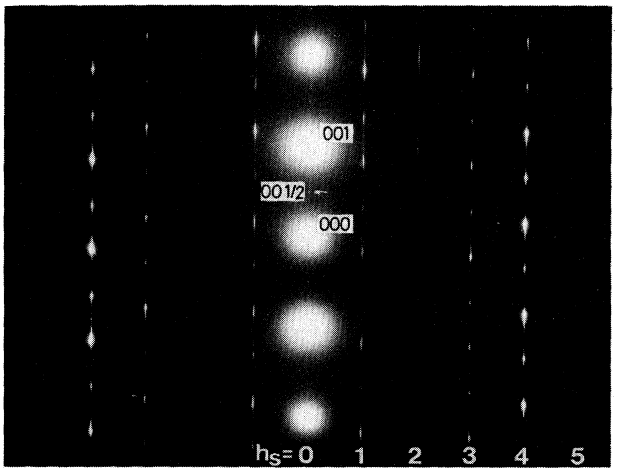

FIG. 14. [140] diffraction pattern of the C phase. The rows of h_s (=0,1,2,3,4,5) mean that of $h_s\mathbf{q}^p_{C1}$, i.e., indices with subscript of s, have the base vectors $\mathbf{q}^p_{C1}$ and $\mathbf{q}^p_{C2}$ in the basal plane, and ξ is a coordinate in the unit of $|\mathbf{c}^*|$.

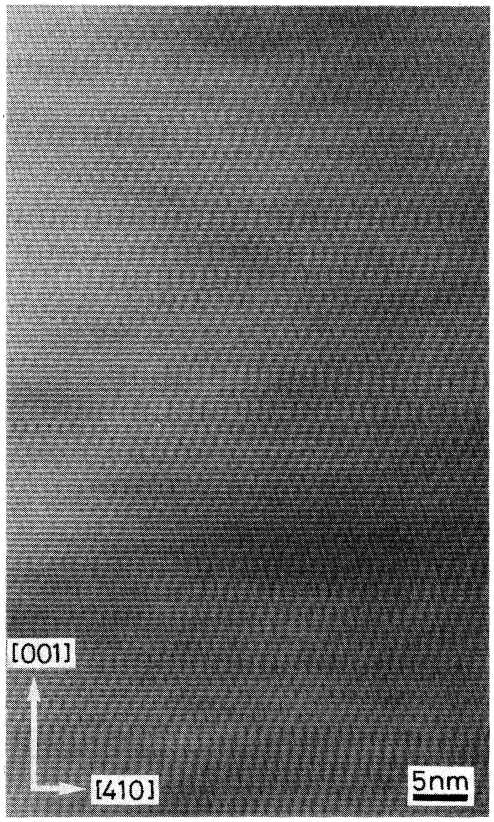

FIG. 15. [140] high-resolution image of the C phase at 90 K.

the secondary reflections, while the others are the primary reflections which are independent from each other (Fig. 11). The intensity distribution of these primary reflections are similar to the result obtained by an x-ray diffraction experiment by Tanda *et al.*[15] Another important feature of the diffraction pattern is the existence of weak, spotty reflections in the middle of any two neighboring 0,0,l reflections where l is an integer. These weak reflections are not due to the double diffraction effect, as they are also observed in the [010] diffraction pattern in which it is impossible to produce the double diffraction effect. The existence of $0,0,l+\frac{1}{2}$ reflections suggests that the stacking order of the commensurate phase has a period of two c_0.

In Fig. 15, we show a high-resolution image corresponding to the diffraction pattern of Fig. 14. The dark bands in this figure correspond to atomic layers and the black dots in them correspond to the images of rows of clusters. Almost all of the stacking have a unit of double layers connected by the stacking vector of **c** without a stacking shift. In order to clarify this stacking order and to reproduce the diffraction pattern, we made a model of the stacking by reading the location of clusters from this image. Thirteen possible transitional components of stacking vectors (cf. Fig. 12) were chosen in the basal plane[27] and the lattice parameters $c_0=0.5919$ nm and $a_0=0.3356$ nm, were assumed.[28] Based on these numbers, the angle between the c axis and the vector connecting one cluster to another one of the next layer was calculated. The following 156 stacking orders were obtained from the image:

0,7,0,8,0,11,0,11,0,11,11,7,0,8,0,7,0,7,0,8,0,8,0, 8,0,8,0,11,0,11,0,11,0,11,
0,11,0,8,0,7,0,7,0,8,0,8,0, 11,0,8,0,11,0,8,0,7,0,7,0,7,0,7,0,11,0,11,0, 11,0,
11,0,11,0,7,0,7,0,11,0,8,0,11,0,8,0,8,0,11,0 11,0,11,0,11,0,7,0,7,0,11,0,8,0,
11,0,8,0,11,0,11,0,8,0, 11,0,11,0,11,0,7,0,7,0,7,0,8,0, 11,0,8,0, 11,0,7,0,
8,0,11,0,11,0,11,0,7,0,7,0,7,0,7,0,8,0,8,0.

These numbers correspond to the translation vectors in Fig. 12 (the number 7, for example, indicates the stacking shift corresponding to 0 to 7 in Fig. 12, and 0 indicates no stacking shift). The stacking vector is such a translation vector plus **c**. Here, only four types of translation vectors appear, i.e., 0, 7, 8, and 11, and almost all of the stacking has a unit of the double layers except only one in 156. The stacking sequence of double layers is essentially disordered as mentioned by Nakanishi and Shiba.[27] But, in this observation, we can see two types of stacking patterns. One is the sliding stacking such as repetitive 11,0,11,0,... with the repetition of $6c_0$ to $10c_0$. The other

stacking pattern is a local screw stacking indicated by the underlined portion such as 11,0,7,0,8,0,... .

Based on this observation, we calculated the structure factor and the intensity distribution by assuming that each cluster has a constant form factor of $\frac{1}{156}$. Figures 16(a), 16(b), and 16(c) show the intensity profiles along $1_s,0_s,\zeta$; $\bar{1}_s$, $1_s,\zeta$; and $0_s,\bar{1}_s,\zeta$ respectively, where ζ is a coordinate in the unit of $|\mathbf{c}^*|$ in the reciprocal space and first two digits with subscript "s" are indices in terms of the cell spanned by $\mathbf{q}^P_{C1}$ and $\mathbf{q}^P_{C2}$ (Fig. 11). Overall features of these profiles are similar to one another and are comparable to the x-ray result taken by Tanda and Sambongi.[20] But fine details are different, for example, the location of the maximum indicated in the figure. Therefore there is no threefold symmetry in the stacking, and this is consistent with the [001] high-resolution observation (Fig. 13). Figure 16(d) shows the average of the three independent profiles shown in 16(a)–16(c). The maximum points at 0.314 and 0.814 are close to the x-ray results of 0.310±0.003 and 0.825±0.003.[20] However, the diffraction pattern (Fig. 14) may have to be reexamined if the intensity of each streak has fine structures. These differences in the detail of the profile in the intensity distribution are, however, mainly due to the difference in statistics, because the size of the area of the observation in the high-resolution image, that of diffraction pattern, and that of x ray are about 100 nm, 1 μm, and 100 μm, respectively.

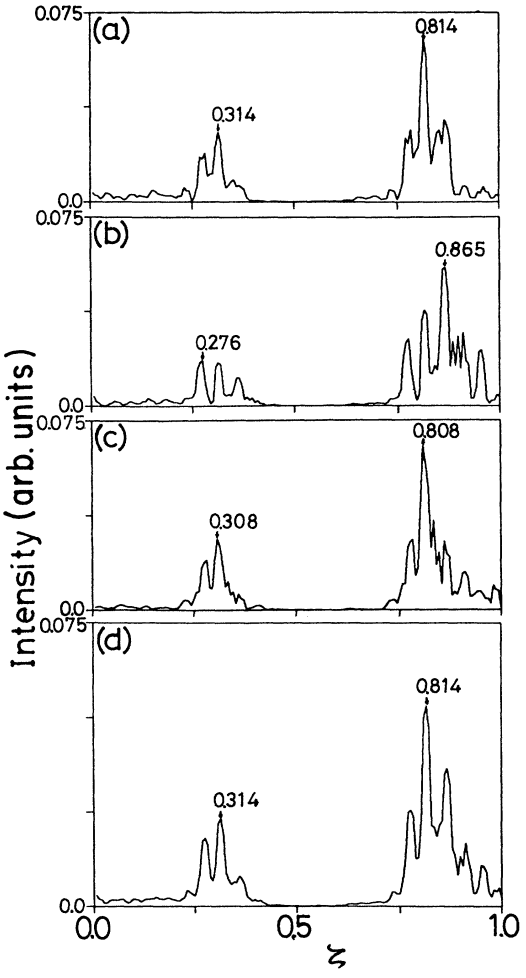

FIG. 16. Calculated intensity profiles based on the stacking sequence obtained from the [140] high-resolution image of the C phase (Fig. 15) (a) along $1_s,0_s,\zeta$; (b) along $\bar{1}_s,1_s,\zeta$; (c) along $0_x\bar{1}_s,\zeta$. Here, the digit with "s" is the index based on the rhombus spanned by $\mathbf{q}^P_{C1}$ and $\mathbf{q}^P_{C2}$ (Fig. 11). (d) Average of (a), (b), and (c).

As mentioned before, the commensurate structure has weak reflections at $0,0,l+\frac{1}{2}$. The calculated intensity based on the stacking model used does not give any intensity at $0,0,l+\frac{1}{2}$, because we assumed that the stacking period along the c axis was the same as $|c_0|$ and the unit of form factor of cluster was constant. The stacking of the commensurate phase, however, has a unit of double layers. Therefore, within the double layer, there can be a particular interaction.[29,30] Such an interaction may change the lattice spacing along the c axis of the double layer[28] and also the form factor of the cluster. From observations on the C phase, it can be said that this phase is commensurate in the basal plane, but, essentially, is not commensurate in three dimensions because the stacking order of the C phase is not periodic.

E. The T phase and the NC phase on warming

In Fig. 17, changes of diffraction patterns with temperature taken from the direction perpendicular to the c axis are shown. Because of the diffraction spots rotated around the $\mathbf{c}^*$ axis, the direction of the incident beam was chosen to excite three independent primary spots at the same time. Therefore the beam was tilted a little from the [140] direction. The characteristics of diffraction spots in the T phase [Figs. 17(a) and 17(b)] are that the direction of the streaks is tilted from the direction of the c axis. This fact is consistent with the intensity distribution of the secondary spots in the c plane [Figs. 4(f) and 4(g)] and also indicates that the long-range ordering in the c plane is missing. On the other hand, the primary spots in the NC phase on warming [Fig. 17(c)] are rather spotty and this is also consistent with the [001] diffraction pattern shown in Fig. 4(h).

We also measured the relative separation of the independent primary spots from the $\mathbf{a}^*$-$\mathbf{b}^*$ plane along the $\mathbf{c}^*$ direction with respect to the unit reciprocal layer distance (ζ in the $|\mathbf{c}^*|$ unit). The temperature dependence of ζ is thus shown in Fig. 18. The most important features here are that ζ in the T phase deviates from $\frac{1}{3}$, tends to approach $\frac{1}{3}$ as the temperature is raised, and in the temperature range of the NC phase ζ, reaches $\frac{1}{3}$ within the experimental error. The deviation of ζ from $\frac{1}{3}$ in the T phase was first pointed out by Tanda *et al.*, but the amount of the deviation in their experiment is larger than the results shown here. The change in ζ at the boundary of the T phase and the NC phase on warming at 280 K is discontinuous, and it is believed that this discontinuous change in ζ and the endothermic peak in the specific heat measurements[11,22] are related.

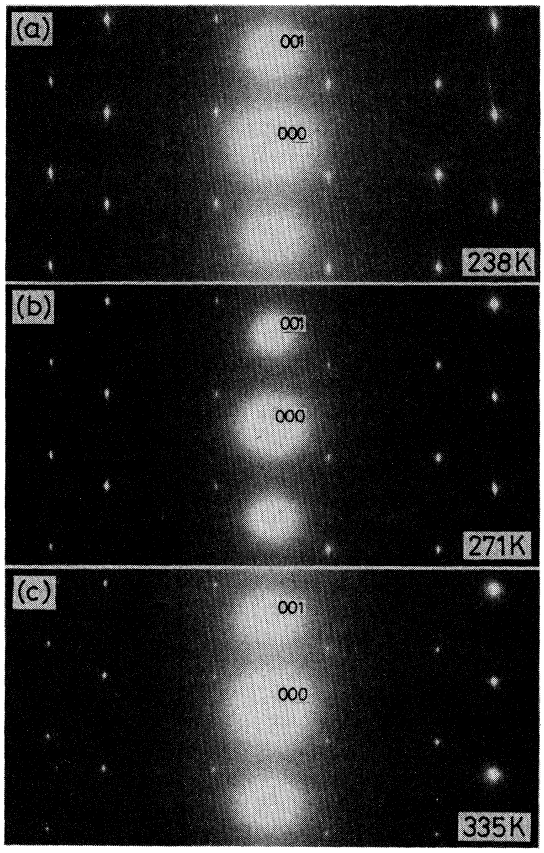

FIG. 17. (a) and (b) Diffraction pattern of T phase on warming; (c) diffraction pattern of NC phase on warming. The incident directions are chosen to excite three independent primary spots.

In Fig. 19, a typical high-resolution image of the T phase taken from the direction perpendicular to the c axis is shown. Here, fringes that correspond to the primary spots around 000 are very wavy and the double-layer substructure that is characteristic of the C phase (Fig. 15) is not visible anymore. If one marks every third black dot along the c axis, the orientation of these marks has a fluctuation and the averaged orientation of the dotted line connecting these black dots on every third layer deviates from the orientation of the c axis. On the other hand, a typical high-resolution image in the NC phase on warming is shown in Fig. 20. Although there is also a very small fluctuation in the fringes corresponding to the elongation of the primary spot, the dotted lines, created in the same way as above, are along the c axis. This proves that, in the T phase, the stacking deviates from that of $\frac{1}{3}$, but, in the NC phase, the $\frac{1}{3}$ stacking is taken. This is consistent with the behavior of ζ shown in Fig. 18.

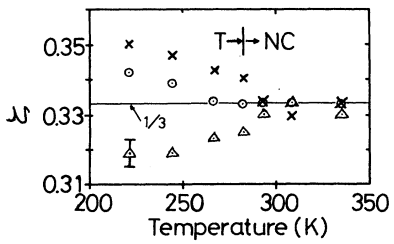

FIG. 18. Temperature dependence of the ζ (in units of $|\mathbf{c}^*|$) of three independent primary spots on warming in the T and the NC phase.

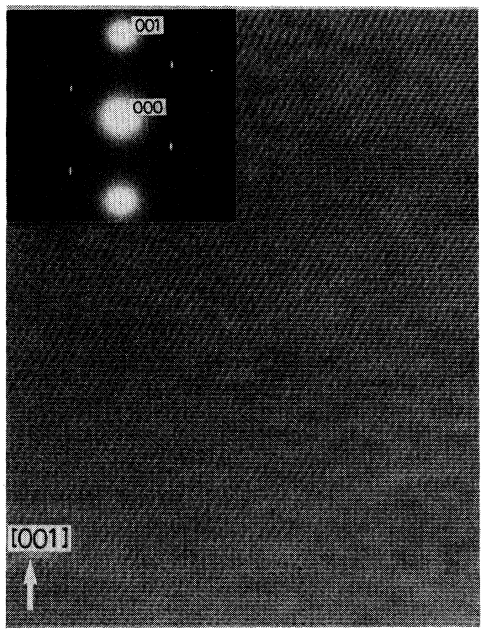

FIG. 19. High-resolution image and diffraction pattern of the T phase at 226 K. The direction of the incident beam is chosen so as to excite a pair of primary spots around 000.

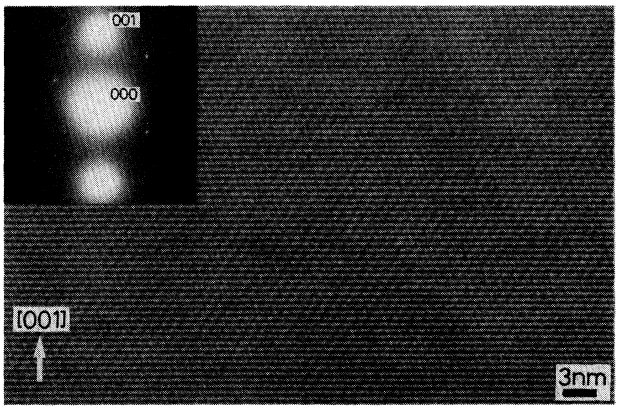

FIG. 20. High-resolution image of the NC phase at 301 K on warming and the corresponding diffraction pattern. The direction of the incident beam is chosen so as to excite a pair of primary spots around 000.

Observations with the incident beam along the c axis, however, show an essential difference in character from those on cooling. Figure 21(a) shows a [001] high-resolution image of the T phase and an optical diffractogram by a laser Fourier-transformation method from this image in order to confirm that this image represents the feature of electron diffraction pattern of the T phase. The optical diffraction pattern gives the value of $|\mathbf{q}^P|/|\mathbf{a}^*|=0.2817\pm0.001$, which agrees with the value obtained by electron diffraction (Fig. 3). In the image, an assembly of discontinuous lines that connects the high-intensity white dots with the period of the commensurate structure in the c plane can be detected. Generally speaking, the understanding of high-resolution image is difficult in the case in which the structure is complex along the projected direction, because the contrast is given as a result of phase modulation caused both by the material and by the focus condition of the objective lens. But, in general, the local periodic information and the symmetry are retained in the image. For example, the [001] high-resolution image of the C phase (Fig. 13) can be understood by the repetition of the same pattern with the size of the unit cell shown in Fig. 12, even if the structure of the C phase has a disordered stacking along the projected direction. In the T phase, such a discontinuity from one commensurate domain to another was observed on the surface by STM (Ref. 21) and was interpreted by the concept of discommensuration: an assembly of domains of commensurate structure connected by phase slip regions.

Based on the concept of discommensuration, we first selected the assembly of strong white spots from Fig. 21(a) and then tried to select regions of the commensurate structure in the c plane. By selecting such strong white dots, it is possible to see an assembly of local hexagonal networks. Selected dots from the image of Fig. 21(a) are thus mapped in Fig. 21(b), in which domains of hexagonal networks connected to each other by the translational vectors of 7,8,11 or 2,5,6 in Fig. 12 are obtained. These combinations of three vectors are the stacking vectors on the c plane of the C phase. Some parts of domain boundaries thus constructed show an overlapping of domains, because this image shows the projected structure along the c axis, but such overlapping parts are not larger than the size of domains.

The length of these projected stacking shift vectors is shorter than the length of the unit vector $|\mathbf{a}_c|$, and these vectors are rotated from the fundamental direction of the commensurate structure. Therefore the variation of the $|\mathbf{q}^P|/|\mathbf{a}^*|$ and ϕ with temperature on warming process can be easily explained if the density of such two-dimensional discommensuration increases with temperature.

Figure 22(a) shows a [001] high-resolution image of the NC phase on warming which shows similar features to that of the T phase [Fig. 21(a)]. The optical diffractogram in the inset indicates that more rotation has taken place compared to that of the T phase and the

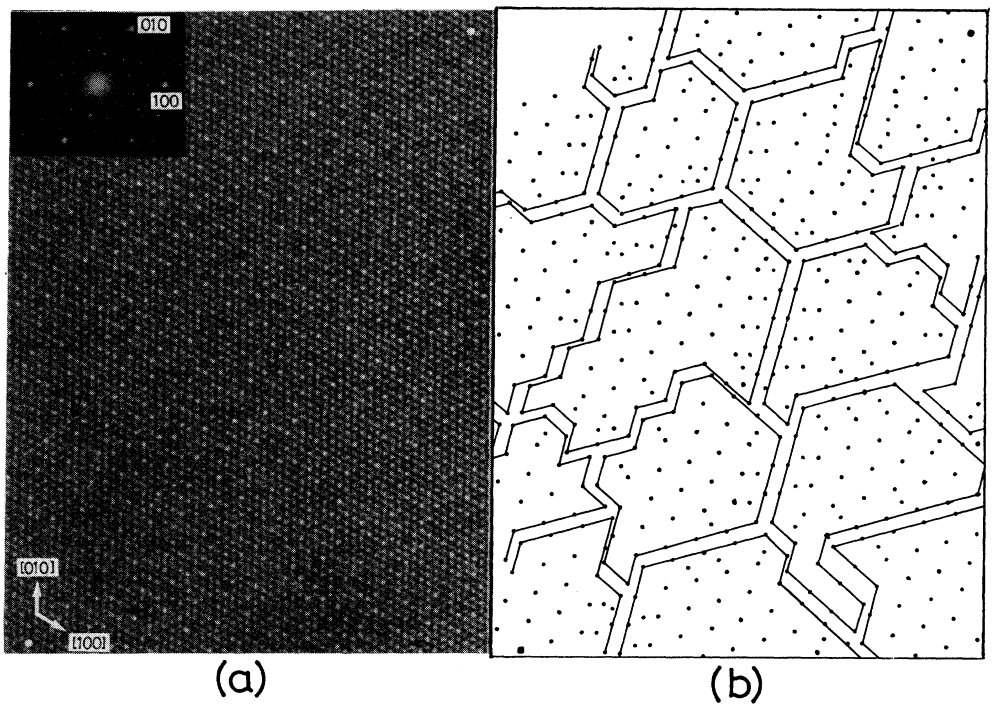

FIG. 21. (a) [001] high-resolution image of the T phase at 226 K and corresponding optical diffraction pattern taken from the same area. (b) Domain structure of the T phase. Hexagonal network is traced from the image of (a) by taking the brightest spots into account. The domains enclosed by lines represent domains with the commensurate structure, even though there are some extra spots due to the overlapping of domains. Large white dots at the corners of (a) and large black dots in (b) indicate the same position.

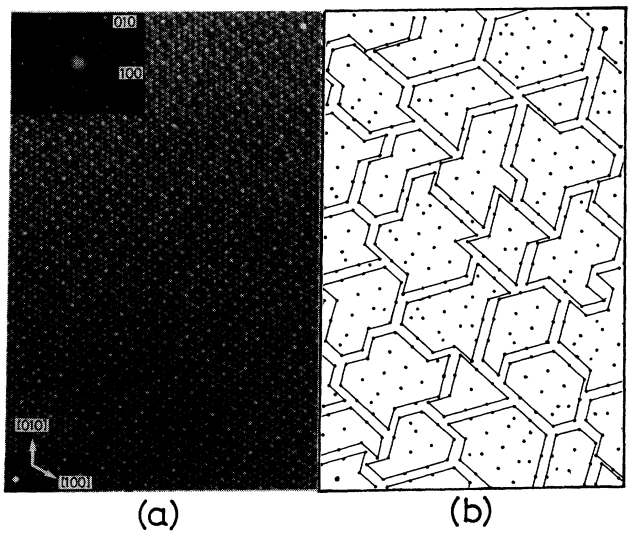

FIG. 22. (a) [001] high-resolution image of the NC phase on warming at 301 K and the corresponding optical diffraction pattern. (b) Domain structure of the NC phase on warming. This is created from the image of (a) by the same way as Fig. 21(b) is created from Fig. 21(a).

value of $|\mathbf{q}^P|/|\mathbf{a}^*|$ obtained by this optical diffractogram is 0.2845 ± 0.001. This is also consistent with the results of the electron diffraction studies (Fig. 3). Similar to the case of the T phase, it is possible to divide the image into small commensurate domains as shown in Fig. 22(b). The size of these domains in the NC phase on warming is much smaller than that in the T phase at 226 K (Fig. 21). It should be emphasized that the NC phase on warming at 301 K has also discommensurate networks, while the NC phase on cooling does not have such discommensuration networks.

On warming from the C phase, the mechanism of rotation and the change of the period in the c plane has the same character both in the T phase and the NC phase. On the other hand, the difference between the T phase and the NC phase on warming is characterized by the difference in the stacking order as shown in Fig. 18. The deviation from the threefold symmetry in the C phase is due to a statistical deviation from the periodic arrangement in the three stacking vectors. But, whether the deviation from the threefold symmetry in the T phase has similar statistical origin to that in the C phase is not clear at this moment.

IV. DISCUSSION AND CONCLUSION

The series of observations described above reveals that the phase transformations in $1T$-TaS_2 have a large hysteresis depending on the previous thermal history. On cooling from the IC phase, the NC phase has characteristics similar to that of the incommensurate structure in the basal plane, with the stacking order of $\frac{1}{3}$. In other words, it retains the structural nature similar to that of the IC phase from where it is derived. The C phase has the stacking which also deviates from that of $\frac{1}{3}$ and, at the same time, shows the existence of stacking disorder. In addition, the C phase has a specific double stacking in every second layer. On the other hand, on warming from the C phase, the T phase appears first. Here, the basal plane consists of domains of the commensurate structure separated by a network of discommensuration. In the T phase, the stacking deviates from that of $\frac{1}{3}$ and tends to approach that of $\frac{1}{3}$ as the temperature is raised. The NC phase follows the T phase on warming. Here, a domain structure with discommensurate network similar to that of the T phase exists and the size of each domain is even smaller. As a result, the decrease in the size of the domain with temperature gives a natural explanation of the change of ϕ and $\mathbf{q}^P$ with temperature (Figs. 2 and 3). One difficulty is to explain why and how the stacking approaches $\frac{1}{3}$ with temperature. So far, it is only recognized that the stacking vectors have a statistical deviation from $\frac{1}{3}$ in the T phase, but the details are not clear.

In systems that show a large temperature hysteresis such as $1T$-TaS_2, it is important to choose the initial state and a fixed thermal history in taking data in order to obtain consistent results. Phase transformation in the case of $2H$-$TaSe_2$ also shows a hysteresis which was confirmed by the x-ray experiment.[31] This situation is qualitatively similar to the case of $1T$-TaS_2, and the existence of the hysteresis had created a controversy in interpreting the discommensuration structure.[3–7] Therefore it is important to take into account the thermal history in comparing data in discussing the phase transformation of $1T$-TaS_2. As explained earlier, we choose the IC phase as the initial state. This was also the choice of Bayliss, Ghorayeb, and Guy[22] and Sezerman, Simpson, and Jericho[9] for their measurements of macroscopic properties of $1T$-TaS_2. Their results also revealed the existence of the T phase on warming and the differences in the NC phases on cooling and on warming. Our observations are consistent with their results. On the other hand, Tanda *et al.*,[15] in their x-ray experiments, chose the NC phase at room temperature as the initial state in their x-ray experiment, because the stacking property was the same, being equal to $\frac{1}{3}$, in the NC phase both on cooling and warming. They reported for the first time the existence of the T phase with long narrow domain structures, which was also confirmed by a STM experiment.[21] Their results are qualitatively the same as that of ours in the sense that the T phase has a structure with discommensurate network and does not have a threefold symmetry. However, there are also some qualitative differences. For example, differences exist in the relative height of three independent primary spots in the unit reciprocal layer distance, in the shape of the discommensuration network and in the phase slip among domains at the discommensuration.

The change of ϕ and $|\mathbf{q}^P|/|\mathbf{a}^*|$ with temperature on warming, as shown in Figs. 2 and 3, can be understood if the size of domains having the commensurate structure decreases and if the relative area of discommensurated networks increases with temperature as shown in Figs. 21 and 22. The geometrical relation between the size of

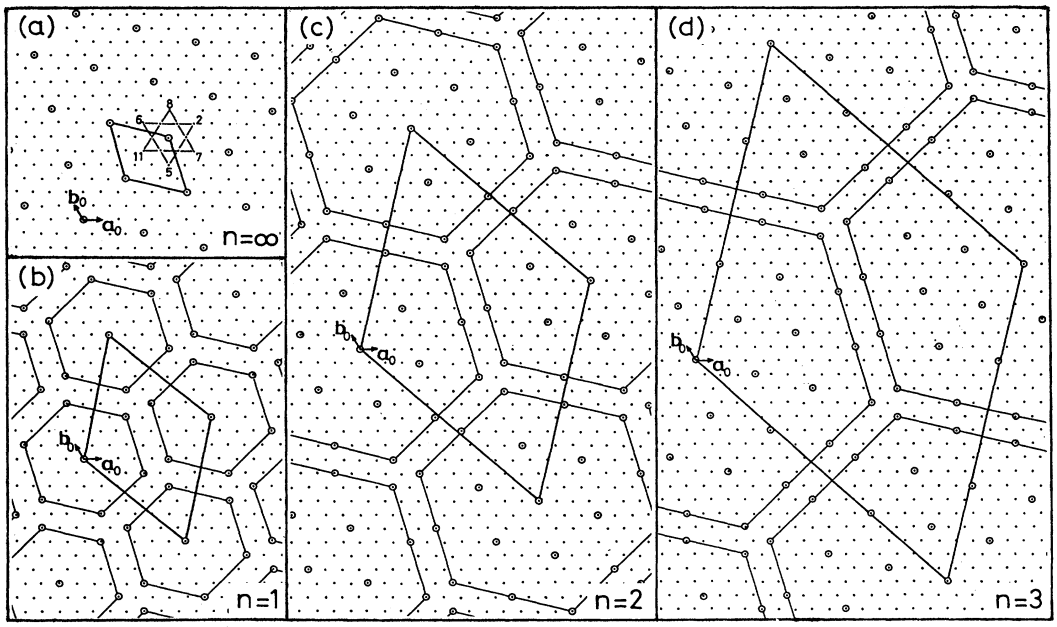

FIG. 23. Idealized model for discommensuration network. (a) The C phase. The mark ○ indicates the location of the star-shaped cluster of the phase and the number indicates the location of the center of the star-shaped cluster for possible stacking positions. (b) Arrangement of hexagonal commensurate domains of the size $n=1$ (the length of the side of the hexagon of the commensurate domain is characterized by the size of the rhombus of the unit cell of the commensurate structure) arranged with relative shifts of 8, 7, and 11 (this is equivalent to the shift of 5, 6, and 2). (c) Discommensurate arrangement of hexagonal commensurate domains with size $n=2$. (d) Discommensurate arrangement of hexagonal commensurate domains with size $n=3$.

commensurated domains and the relative area of discommensurated networks can be calculated if one idealizes the discommensuration model based on Figs. 21 and 22 in the following fashion. As is shown in Fig. 23, hexagonal commensurate regions with various sizes can be represented by the number n. Here, n indicates the size of the hexagon (by the length of the edge) in terms of the size of the unit cell of the C phase (equal to $|3\mathbf{a}_0-\mathbf{b}_0|$) as indicated in Fig. 23(a). An idealized discommensurate state can be realized by arranging these hexagonal commensurate regions regularly with phase slips 8, 7, and 11 (5, 6, and 2 are equivalent). As the size of the hexagon decreases to $n=1$ ($n=\infty$ corresponds to the commensurate phase), the relative area of the discommensuration networks increases. Then, the relation between n and ϕ and $|\mathbf{q}^P|/|\mathbf{a}^*|$ can be calculated as

$$\phi_n=\frac{180}{\pi}\tan^{-1}\left[\frac{\sqrt{3}n}{7n+2}\right],$$

$$\frac{|\mathbf{q}_n^P|}{|\mathbf{a}^*|}=\frac{2(3n+1)}{\{3[(3n)^2+3(7n+2)^2]\}^{1/2}}.$$

In Fig. 24, $|\mathbf{q}_n^P|/|\mathbf{a}^*|-\phi_n$ thus represents a straight dotted line and $n=\infty$ corresponds to the C phase. The relation $|\mathbf{q}^P|/|\mathbf{a}^*|-\phi$ for the experiment can be obtained from Figs. 2 and 3 and is plotted in Fig. 24 by open circles (on cooling) and solid circles (on warming). It is clear from the plot that, in the NC phase on cooling, ϕ

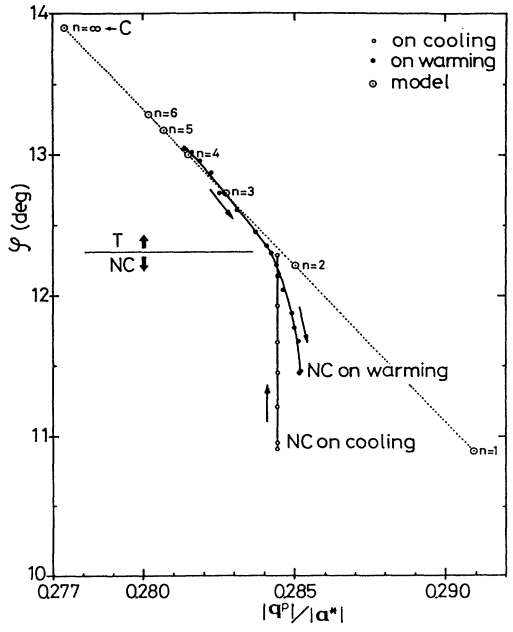

FIG. 24. Relation between $|\mathbf{q}^P|/|\mathbf{a}^*|$ and ϕ. Open circles indicate the change on cooling from the IC phase, while solid circles indicate the change on warming. The dotted line indicates the relation $|\mathbf{q}^P|/|\mathbf{a}^*|-\phi$ calculated from the idealized model of the discommensurate network.

increases linearly and intersects the dotted line at 12.3°, where it transforms into the C phase. On warming, the change of ϕ and $|\mathbf{q}^P|/|\mathbf{a}^*|$ is along the dotted line represented by the idealized discommensuration model. The transformation from the T phase to the NC phase is continuous and the relation gradually deviates from the dotted line of the idealized model. Here, the discontinuity at $\phi=12.3°$ does not appear clearly. However, the idealized model is concerned with the discommensuration only in the c plane and the effect of the change of the stacking order is not included. This type of the idealized model would only be valid for the case where n is large.

The behavior of the transformation in $1T$-TaS_2 on warming thus has become very clear with the help of Figs. 21 and 22, except for the effect of stacking order. Although it was possible to determine the stacking order in the C phase by high-resolution electron microscopy, in the discommensurate structure, reliable observations could not be made because the observation is an average over a number of commensurate domains. Therefore, at this moment, we can only safely say that the stacking order in the T phase deviates from that of $\frac{1}{3}$ while in the NC phase, it is approximately that of $\frac{1}{3}$. The effect of this change to $|\mathbf{q}^P|/|\mathbf{a}^*|$ is not quite clear.

On cooling, on the other hand, the rotation of ϕ with temperature takes place with $|\mathbf{q}^P|/|\mathbf{a}^*|$ almost constant without producing the discommensuration. With the value of a_0 (the size of the unit cell) obtained from the x-ray measurement,[28] the absolute value of $|\mathbf{q}^P|$ is estimated to be

$$|\mathbf{q}^P|=9.780\ \text{nm}^{-1} \quad \text{at 350 K}$$

and

$$|\mathbf{q}^P|=9.781\ \text{nm}^{-1} \quad \text{at 190 K}$$

in the NC phase on cooling. In other words, $|\mathbf{q}^P|$ does not change on cooling. The change in the NC phase on cooling is purely a rotation of $\mathbf{q}^P$ and a discommensuration in the ordinary sense does not exist. At lower temperatures, the NC phase transforms into the C phase by a first-order phase transition. The rotation of $\mathbf{q}^P$ in the NC phase can thus be interpreted as a tendency of the NC phase to approach the C phase.

Based on our results, the nature of the NC phase and the IC phase is essentially the same. However, in the IC phase, no rotation of the q vector is observed and there is a discontinuous rotation of the q vector at the phase boundary between the IC and NC phases. The only way to reconcile these facts is to regard both the IC phase and the NC phase as incommensurate phases with different nesting conditions. Features of the incommensurate-commensurate transition between the NC phase and the C phase have thus been discussed. The features of incommensurate-commensurate transitions in $1T$-TaS_2 are very complicated and it would be necessary to accumulate much more information on electronic structures of this substance before we can explain the characteristics of the phase transitions in a much more systematic fashion.

ACKNOWLEDGMENTS

The work was supported by the National Science Foundation, Solid State Physics Program, Grant No. DMR8304314. One of the authors (T.I.) was partially supported by the Kazato Foundation. We also thank Dr. D. Shindo and Mr. Z. P. Zhang for discussions, and Dr. M. Sankararaman for helpful comments on the manuscript.

*On leave of absence from Nagaoka University of Technology, Nagaoka, Niigata 940-21, Japan.

[1]P. M. Williams, G. S. Parry, and C. B. Scruby, Philos. Mag. **29**, 695 (1974).
[2]J. A. Wilson, F. J. Di Salvo, and S. Mahajan, Adv. Phys. **24**, 117 (1975).
[3]C. H. Chen, J. M. Gibson, and R. M. Fleming, Phys. Rev. Lett. **47**, 723 (1981).
[4]C. H. Chen, J. M. Gibson, and R. M. Fleming, Phys. Rev. B **26**, 184 (1982).
[5]K. K. Fung, S. McKernan, J. W. Steeds, and J. A. Wilson, J. Phys. C **14**, 5417 (1981).
[6]T. Onozuka, N. Otsuka, and H. Sato, Phys. Rev. B **34**, 3303 (1986).
[7]Y. Koyama, Z. P. Zhang, and H. Sato, Phys. Rev. B **36**, 3701 (1987).
[8]C. B. Scruby, P. M. Williams, and G. S. Parry, Philos. Mag. **31**, 255 (1975).
[9]O. Sezerman, A. M. Simpson, and M. H. Jericho, Solid State Commun. **36**, 737 (1980).
[10]T. Haga, Y. Abe, and Y. Okamoto, Phys. Rev. Lett. **51**, 678 (1983).
[11]A. Suzuki, R. Yamamoto, M. Doyama, H. Mizubayashi, S. Okuda, K. Endo, and S. Gonda, Solid State Commun. **49**, 1173 (1984).
[12]T. Tani and S. Tanaka, J. Phys. Soc. Jpn. **53**, 1790 (1984).
[13]A. Suzuki, R. Yamamoto, M. Doyama, H. Mizubayashi, and S. Okuda, J. Phys. (Paris) C **10**, 677 (1985).
[14]K. K. Fung, J. W. Steeds, and J. A. Eades, Physica B **99**, 47 (1980).
[15]S. Tanda, T. Sambongi, T. Tani, and S. Tanaka, J. Phys. Soc. Jpn. **53**, 476 (1984).
[16]W. L. McMillan, Phys. Rev. B **14**, 1496 (1976).
[17]K. Nakanishi and H. Shiba, J. Phys. Soc. Jpn. **43**, 1839 (1977).
[18]K. Nakanishi, H. Takatera, Y. Yamada, and H. Shiba, J. Phys. Soc. Jpn. **43**, 1509 (1977).
[19]Y. Yamada and H. Takatera, Solid State Commun. **21**, 41 (1977).
[20]S. Tanda and T. Sambongi, Synth. Met. **11**, 85 (1985).
[21]R. E. Thomson, U. Walter, E. Ganz, J. Clarke, A. Zettl. P. Rauch, and F. J. Di Salvo, Phys. Rev. B **38**, 10 734 (1988).
[22]S. C. Bayliss, A. M. Ghorayeb, and D. R. P. Guy, J. Phys. C **17**, L533 (1984).
[23]J. Van Landuyt, Physica B **99**, 12 (1980).
[24]G. Salvetti, C. Roucau, R. Ayroles, H. Mutka, and P. Molinie, J. Phys. Lett. (Paris) **46**, L507 (1985).

[25]M. Kuwabara, M. Tomita, H. Hashimoto, and H. Endoh, Phys. Status Solidi A **96**, 39 (1986).
[26]R. Brouwer and F. Jellinek, Physica B **99**, 51 (1980).
[27]K. Nakanishi and H. Shiba, J. Phys. Soc. Jpn. **53**, 1103 (1984).
[28]F. L. Givens and G. E. Fredericks, J. Phys. Chem. Solids **38**, 1363 (1977).
[29]M. Naito and S. Tanaka, J. Phys. Soc. Jpn. **53**, 1217 (1984).
[30]M. Naito, H. Nishihara, and S. Tanaka, J. Phys. Soc. Jpn. **53**, 1610 (1984).
[31]R. M. Fleming, D. E. Moncton, D. B. McWhan, and F. J. Di Salvo, Phys. Rev. Lett. **45**, 576 (1980).

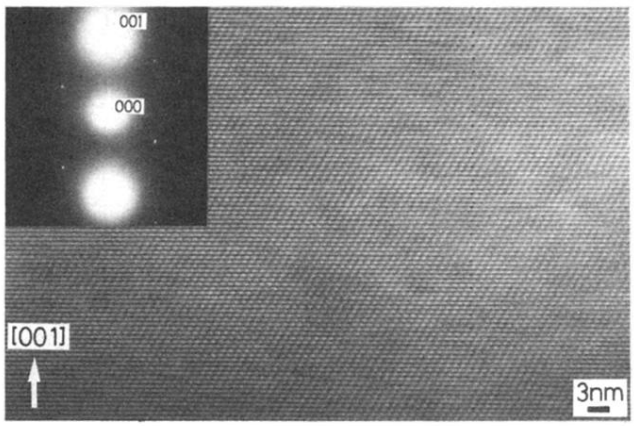

FIG. 10. High-resolution image of the NC phase on cooling at room temperature. The observed direction is perpendicular to the *c* axis, exciting a pair of primary spots.

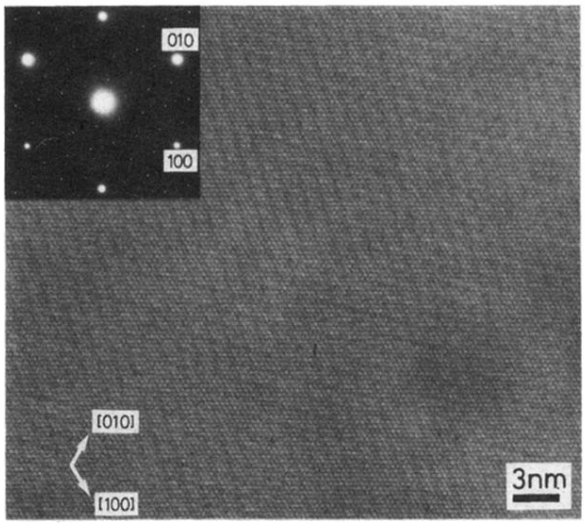

FIG. 13. [001] high-resolution image of the *C* phase at 90 K and a corresponding diffraction pattern.

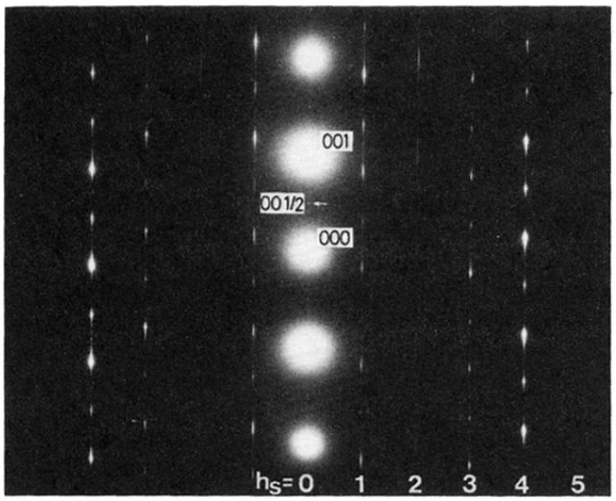

FIG. 14. [140] diffraction pattern of the C phase. The rows of h_s (=0,1,2,3,4,5) mean that of $h_s\mathbf{q}^{\rho}_{C1}$, i.e., indices with subscript of s, have the base vectors $\mathbf{q}^{\rho}_{C1}$ and $\mathbf{q}^{\rho}_{C2}$ in the basal plane, and ζ is a coordinate in the unit of $|\mathbf{c}^*|$.

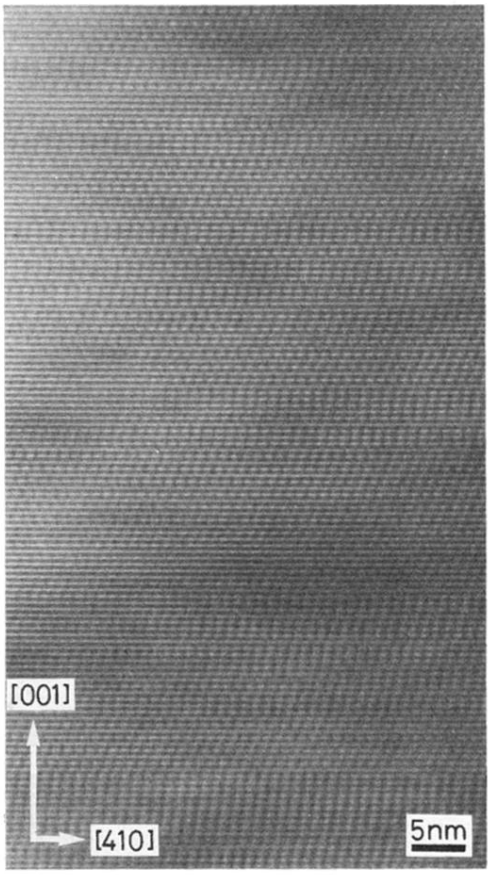

FIG. 15. [140] high-resolution image of the *C* phase at 90 K.

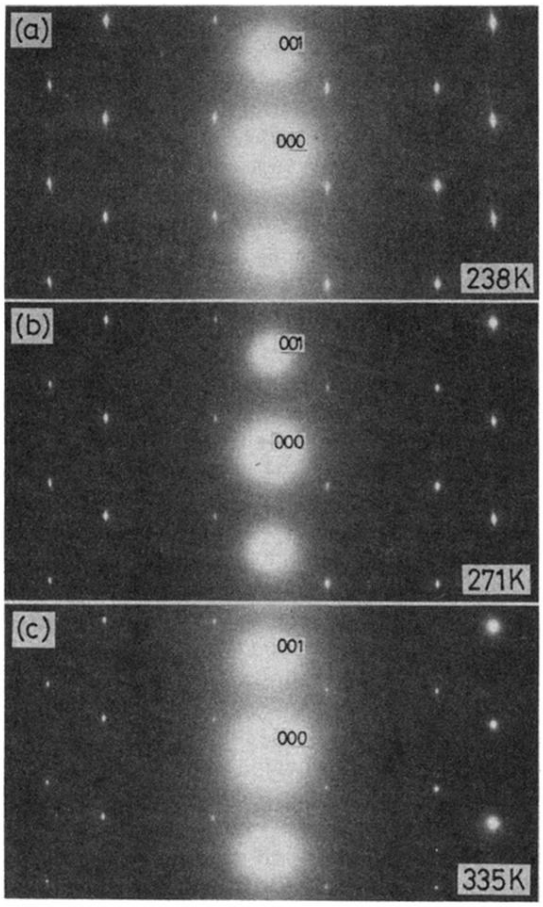

FIG. 17. (a) and (b) Diffraction pattern of T phase on warming; (c) diffraction pattern of NC phase on warming. The incident directions are chosen to excite three independent primary spots.

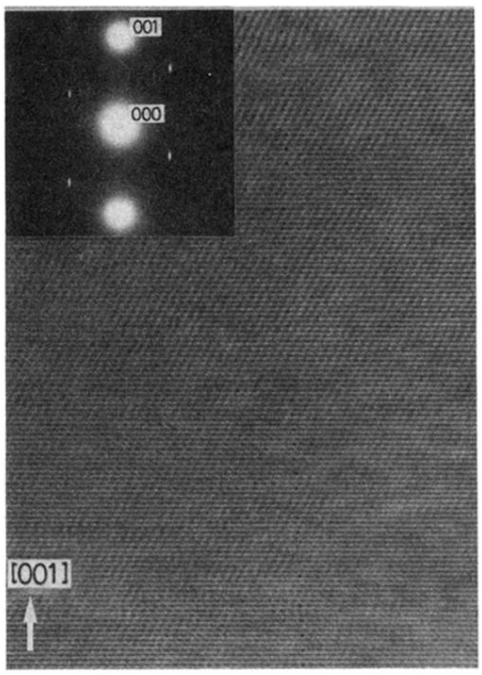

FIG. 19. High-resolution image and diffraction pattern of the T phase at 226 K. The direction of the incident beam is chosen so as to excite a pair of primary spots around 000.

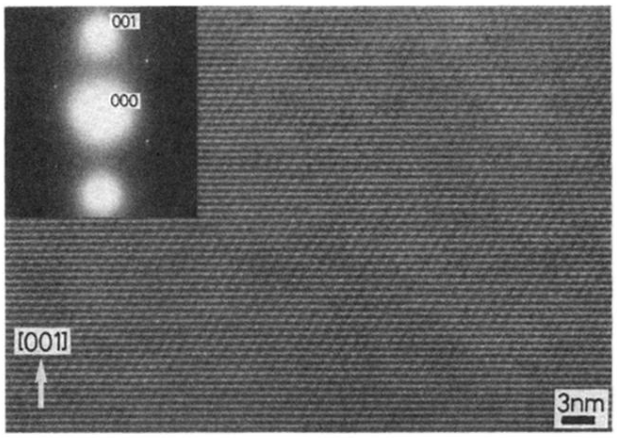

FIG. 20. High-resolution image of the NC phase at 301 K on warming and the corresponding diffraction pattern. The direction of the incident beam is chosen so as to excite a pair of primary spots around 000.

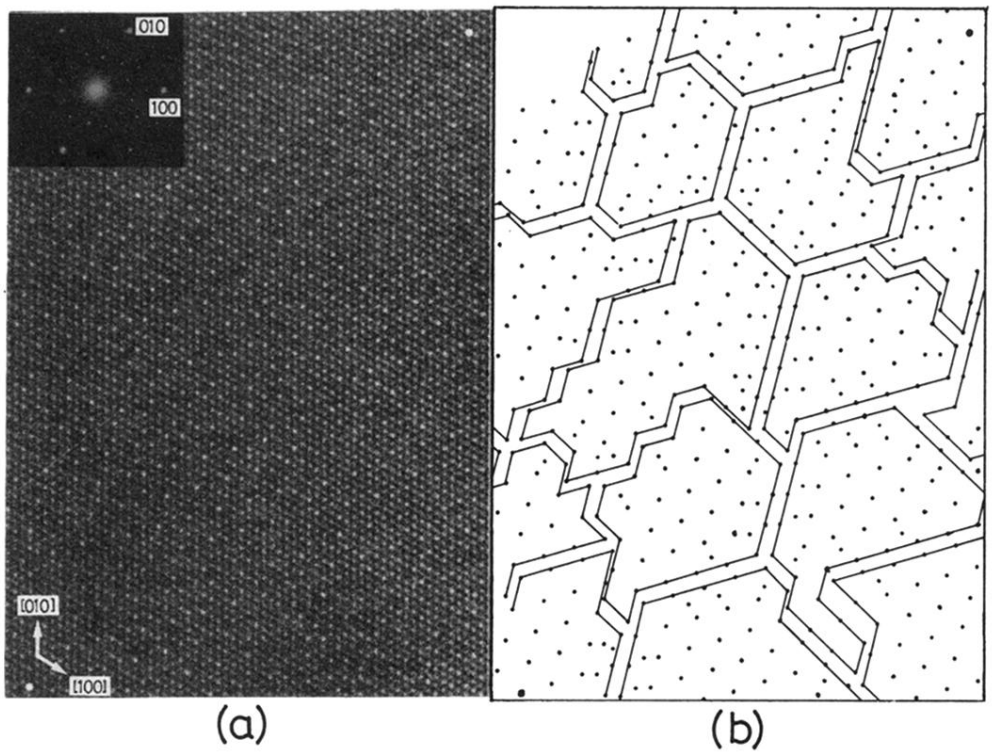

FIG. 21. (a) [001] high-resolution image of the T phase at 226 K and corresponding optical diffraction pattern taken from the same area. (b) Domain structure of the T phase. Hexagonal network is traced from the image of (a) by taking the brightest spots into account. The domains enclosed by lines represent domains with the commensurate structure, even though there are some extra spots due to the overlapping of domains. Large white dots at the corners of (a) and large black dots in (b) indicate the same position.

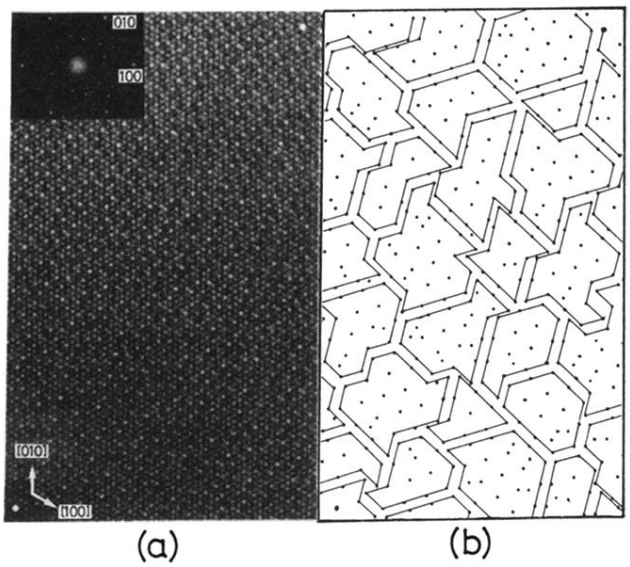

FIG. 22. (a) [001] high-resolution image of the NC phase on warming at 301 K and the corresponding optical diffraction pattern. (b) Domain structure of the NC phase on warming. This is created from the image of (a) by the same way as Fig. 21(b) is created from Fig. 21(a).

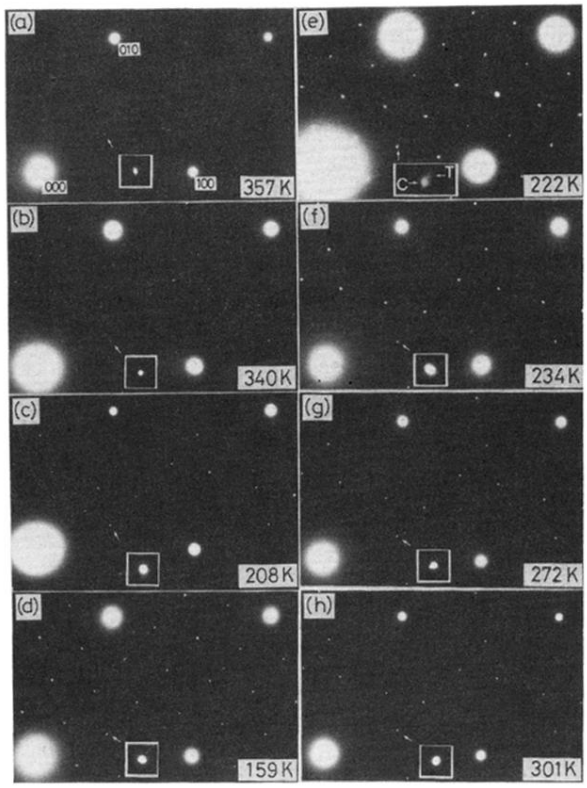

FIG. 4. Temperature variation of the [001] diffraction patterns: (a) the IC phase, (b) and (c) the NC phase on cooling, (d) the C phase, (e) at the transition point from the C phase to the T phase. The splittings of the secondary spots due to the coexistence of the C phase and the T phase are seen. (f) and (g) show the T phase, (h) the NC phase on warming.

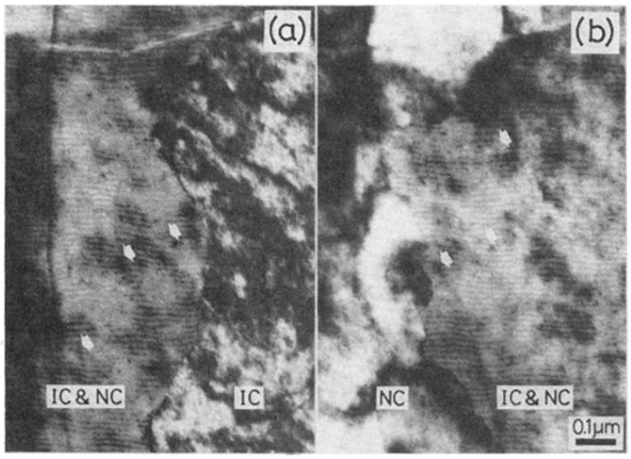

FIG. 6. Dark field images of the phase transformation from the IC phase to the NC phase on cooling. Both (a) and (b) represent the same region. The temperature of (b) is lower than the temperature of (a) by 3°. Because a pair of primary spots of the IC phase and the NC phase are used, the region with moiré fringes corresponds to the coexisting region of the IC phase and the NC phase on cooling.

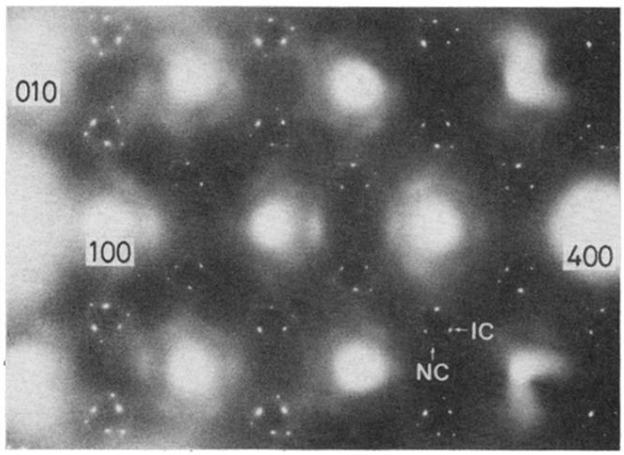

FIG. 8. Diffraction pattern under the 400 Bragg excitation condition taken at the transition temperature from the IC to the NC phase on cooling. Diffuse streaking due to the IC phase appears.

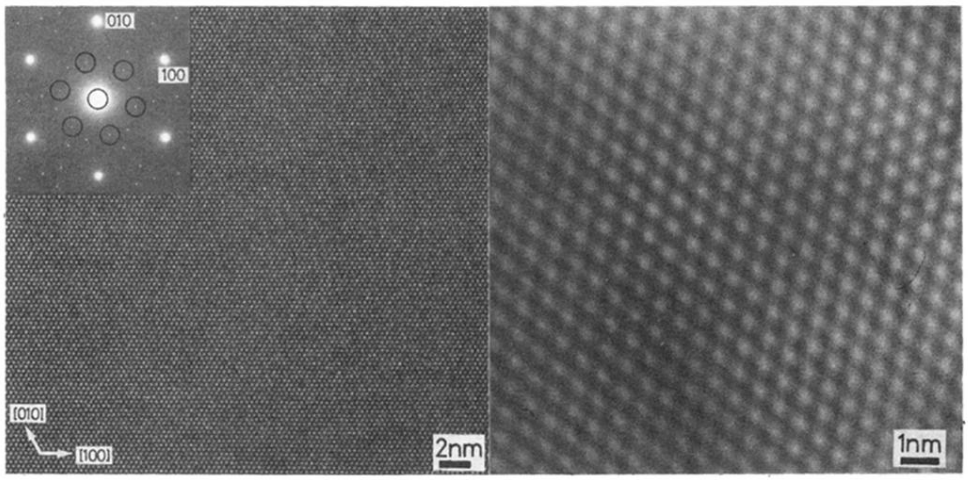

FIG. 9. (a) High-resolution image of the NC phase on cooling at room temperature with the incident beam parallel to [001] and the corresponding diffraction pattern in which the Fourier bandpass used to obtain (b) is shown by circles. In this image, weak incommensurate fringes can be seen. (b) Processed image using a direct spot and six secondary spots.